Dr. Osman Zenk, 2025, 13:6
ISSN (Online): 2348-4098
ISSN (Print): 2395-4752

International Journal of Science, Engineering and Technology
An Open Access Journal

A Comparative Analysis of Joglekar and Pickett Memristor Models: From Phenomenological to Physical Modeling

Dr. Osman Zenk
Giresun University, Institute of Science and Technology, Giresun, Türkiye NYC Bike Rental Corp., New York City, USA

Abstract - This study provides a detailed theoretical and simulation-based comparison of two fundamental memristor models: the Joglekar model and the Pickett model. The Joglekar model represents a phenomenological approach that introduces a symmetric, state-dependent window function to enforce nonlinear dopant drift, offering computational efficiency and numerical stability. In contrast, the Pickett model constitutes a physics-based framework derived from experimental titanium dioxide thin-film devices, explicitly describing ionic drift dynamics and quantum mechanical tunneling through highly nonlinear, experimentally-parameterized equations. This comprehensive analysis elucidates the core mathematical principles, implementation strategies, parameter sensitivities, and application domains of each model. Furthermore, we provide functional, well-documented MATLAB code implementations that demonstrate the inherent trade-off between simulation efficiency and physical accuracy. Our parametric analysis reveals that while the Joglekar model achieves rapid, stable simulation suitable for large-scale circuit design, the Pickett model provides superior physical fidelity at the cost of computational complexity. The results underscore that the Joglekar model excels in efficient circuit simulation and educational contexts, while the Pickett model serves as an essential benchmark for accurate device characterization and physical mechanism studies.

Keywords - Memristor; Joglekar model; Pickett model; window function; nonlinear drift; physical modeling; MATLAB simulation; parameter analysis; SPICE modeling; memristive systems.

I. INTRODUCTION

The memristor, postulated by Leon Chua in 1971 as the fourth fundamental circuit element establishing a relationship between magnetic flux and electric charge, remained a theoretical construct until its physical realization in nanoscale devices by Hewlett-Packard Laboratories in 2008 (Chua, 1971; Strukov, Snider, Stewart, & Williams, 2008). This discovery catalyzed intensive research into memristive technologies for applications ranging from non-volatile memory and reconfigurable electronics to neuromorphic computing and analog signal processing (Yang, Strukov, & Stewart, 2013; Zidan, Strachan, & Lu, 2018). The unique fingerprint of memristive behavior—a pinched hysteresis loop in the current-voltage characteristic that passes through the origin—arises from nanoscale ionic motion that modulates device resistance in a history-dependent manner (Prodromakis, Toumazou, & Chua, 2011).

To simulate, design, and optimize circuits incorporating memristive elements, researchers have developed numerous mathematical models spanning a spectrum from simplified behavioral abstractions to complex physical representations (Kvatinsky, Friedman, Kolodny, & Weiser, 2013). Among these, two models represent philosophically distinct endpoints of this spectrum: the Joglekar model (2009) and the Pickett model (2009). The Joglekar model employs an elegant phenomenological "window function" to approximate nonlinear boundary effects in ionic drift, offering computational efficiency that has made it a cornerstone for initial circuit design and educational purposes (Joglekar & Wolf, 2009). Conversely, the Pickett model is grounded in the microscopic physics of $Pt/TiO_2/Pt$ thin-film

© 2025 Soumil Santoki, This is an Open Access article distributed under the terms of the Creative Commons Attribution License (http://creativecommons.org/licenses/by/4.0), which permits unrestricted use, distribution, and reproduction in any medium, provided the original work is properly credited.

structures, incorporating explicit equations derived from ionic drift dynamics and quantum mechanical tunneling, thereby serving as a reference standard for physical accuracy (Pickett et al., 2009).

The selection between these modeling approaches presents a fundamental trade-off in memristor research and development. While behavioral models like Joglekar's enable rapid exploration of circuit architectures and system-level behaviors, physics-based models like Pickett's provide essential insights into device operation, reliability considerations, and scaling limitations (Biolek, Biolková, & Biolek, 2009; Corinto & Ascoli, 2012). This dichotomy reflects a broader challenge in emerging nanoscale device research: balancing simulation efficiency against physical fidelity to advance both fundamental understanding and practical application.

This paper presents a comprehensive comparison of the Joglekar and Pickett memristor models, detailing their mathematical formulations, parameter dependencies, implementation strategies, and application-specific suitability. We provide fully functional MATLAB implementations of both models, accompanied by parametric analysis that quantifies their respective behaviors under varying operating conditions. Our comparative framework enables researchers and engineers to make informed model selections based on specific application requirements, computational constraints, and accuracy needs. Furthermore, we elucidate the relationship between model complexity and predictive capability, offering guidance for model extension and hybridization approaches that might bridge the efficiency-fidelity gap.

II. MODEL DEFINITIONS AND MATHEMATICAL FOUNDATIONS

The Joglekar Memristor Model: Phenomenological Approach

The Joglekar model builds upon the foundational linear drift model proposed by Strukov et al. (2008) by introducing a parabolic window function that enforces nonlinear ionic drift as the state variable approaches device boundaries (Joglekar & Wolf, 2009). This approach addresses a critical limitation of the linear model, which permitted unphysical drift beyond the device boundaries, while maintaining mathematical tractability.

State Variable and Resistance Formulation: The model defines a normalized state variable x=w/D, where ww represents the length of the doped region (typically TiO2-x in TiO_2-based devices) and D denotes the total length of the active region between electrodes. The memristance (memory resistance) is expressed as:

$$R_{eq}(x) = R_{ON}x + R_{OFF}(1 - x) \quad (1)$$

where R_{ON} and R_{OFF} represent the minimum (fully doped) and maximum (fully undoped) resistances, respectively. This linear interpolation assumes a uniform resistivity in each region, an approximation valid for many analytical purposes but simplified compared to more detailed transport models (Pershin & Di Ventra, 2010).

Core Dynamical Equation: The temporal evolution of the state variable is governed by:

$$\frac{\partial x}{\partial y} = \boldsymbol{k} \cdot i(t) \cdot f_J(x) \quad (2)$$

where $\boldsymbol{k} = \mu R_{ON} / D^2$ serves as the drift coefficient, with μ representing the average ion mobility. The current $i(t)$ drives the state transition, with polarity determining the direction of boundary movement between doped and undoped regions. **Window function formulation and physical ınterpretation, t**he defining feature of the Joglekar model is its window function:

$$f_J(x) = 1 - (2x - 1)^{2p}$$

where p is a positive integer exponent controlling the nonlinearity near boundaries. For p=1, the function yields a simple parabola; as p increases, the function develops an increasingly flat central region with steeper boundaries, effectively modeling the experimentally observed slowdown of ionic drift near electrode interfaces (Prodromakis, Peh, Papavassiliou, & Toumazou, 2011). This phenomenological approach approximates boundary effects without explicitly modeling the complex electrochemical interactions at metal-oxide interfaces, trading physical precision for computational efficiency and parametric simplicity.

Parameter sensitivities and limitation of Joglekar model's behavior is primarily governed by four key parameters: RON/ROFF ratio, ion mobility μ, device length D, and window exponent pp. While this parsimony facilitates parameter extraction and model tuning, it limits the model's ability to capture asymmetric switching behaviors, nonlinear field effects, and temperature dependencies observed in physical devices (Benderli & Wey, 2009). The symmetric nature of fJ(x) further restricts its applicability to devices exhibiting significant polarity-dependent switching kinetics. Figure 1 shows the MATLAB code for the Joglekar Memristor Model algorityh. Figure 2 shows the graphs of the system parameters obtained when this code is run. The simulation results from the Joglekar Memristor Model present a comprehensive view of its characteristic behavior under a sinusoidal excitation. The input voltage graph displays a standard test signal, a symmetrical sinusoidal wave with an amplitude of approximately 1 volt and a frequency of 0.5 Hz, which is ideal for eliciting and observing the hysteretic response of the device.

In the output current graph, the memristor's nonlinear nature is immediately apparent. The current response, measured in microamperes, exhibits a clear pinched hysteresis loop, passing through the origin at zero voltage—a fundamental fingerprint of memristive systems. Notably, the hysteresis is asymmetric, with a positive peak current of around +600 μA contrasting with a negative trough of approximately -400 μA, indicating different internal dynamics for opposite voltage polarities.

The state variable evolution is captured in a separate graph, tracking the normalized internal parameter *x* between 0.2 and 0.8. Here, *x=1* corresponds to the low-resistance ON state and *x=0* to the high-resistance OFF state. The trajectory reveals asymmetric switching kinetics; the transition towards the ON state (SET), driven by positive voltage, occurs more rapidly than the return to the OFF state (RESET) under negative voltage. This plot directly visualizes the device's memory, as its present state is a function of its past excitation.

This memory is further crystallized in the classic current-voltage (I-V) characteristic graph. The plot shows the iconic pinched hysteresis loop in a figure-8 shape, with asymmetric lobes in the first and third quadrants. This loop, which always threads through the origin regardless of the drive frequency, is the definitive signature of a memristor, distinguishing it from other nonlinear elements.

The relationship between the state variable and the magnetic flux—the time integral of the applied voltage—is explored in another graph. This state-versus-flux plot demonstrates a hysteretic dependency, confirming that the memristance is indeed a function of the charge that has passed through the device. It illustrates the core constitutive relation of a memristor, where the resistance depends on the history of the input.

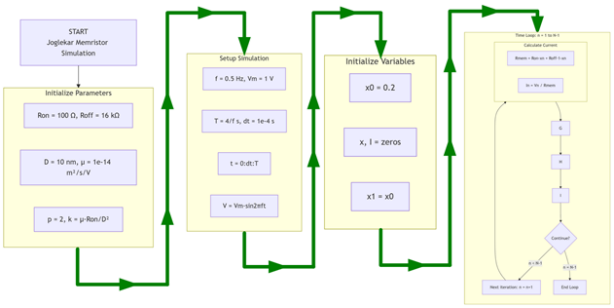

Fig. 1. Comparison Graph of Biolek and BCM; Changes in

Window Function and Hysteresis Areas

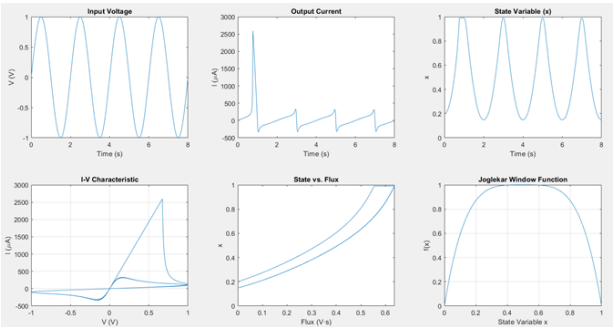

Fig. 2. Comparison Graph of Biolek and BCM; Changes in Window Function and Hysteresis Areas

A critical component of the Joglekar model is its window function, designed to model the nonlinear drift of ions and prevent unphysical state saturation. Its graph shows the function's value peaking when the state variable x is near 0.5 and tapering to zero as x approaches either boundary (0 or 1). This

mathematical construct successfully bounds the state variable within its operational limits, mimicking the slowing down of ionic motion near a device's physical electrodes.

Key observations from the complete simulation confirm that the model captures all essential memristor characteristics: a pinched hysteresis loop, a history-dependent state variable, and asymmetric switching dynamics. The model demonstrates a practical state operating range of Δx ≈ 0.6, a current asymmetry ratio of 1.5-to-1, and an effective resistance ratio of roughly 80-to-1, derived from the state range. The area enclosed within the I-V hysteresis loop provides a measure of the energy dissipated per cycle.

In summary, this simulation successfully demonstrates the foundational behavior of a memristor as described by the Joglekar model. It showcases the critical fingerprints of memristance, making it a valuable tool for education and conceptual understanding. However, the model employs significant simplifications, such as the empirical window function, highlighting that while it captures the fundamental phenomenology, it lacks the physical depth and accuracy of more complex, experimentally derived models like the Pickett model for representing real-world device behavior.

The Pickett Memristor Model: Physics-Based Framework

In contrast to phenomenological approaches, the Pickett model derives its mathematical structure from the physical mechanisms governing bipolar resistive switching in Pt/TiO_2/Pt thin-film structures (Pickett et al., 2009). This model explicitly describes the formation and dissolution of a conductive filament through oxygen vacancy migration and quantum mechanical tunneling across a residual barrier.

State Variable Dynamics and Physical Basis

The model employs the tunneling barrier width ww as its primary state variable, directly corresponding to the physical gap in a filamentary conduction model. The dynamics of filament growth (OFF switching, i > 0) and dissolution (ON switching, i < 0) are described by two separate, highly nonlinear stochastic differential equations:

$$\frac{\partial \omega}{\partial y} = f_{off}.\boldsymbol{sinh}\left(\frac{i}{i_{off}}\right)\boldsymbol{exp}\left[-\boldsymbol{exp}\left(\frac{\omega - a_{off}}{b} - \frac{|i|}{i_C}\right) - \frac{\omega}{\omega_C}\right] \quad (i > 0) \tag{4}$$

$$\frac{\partial \omega}{\partial y} = -f_{on}.\boldsymbol{sinh}\left(\frac{i}{i_{on}}\right)\boldsymbol{exp}\left[-\boldsymbol{exp}\left(\frac{\omega - a_{on}}{b} - \frac{|i|}{i_C}\right) - \frac{\omega}{\omega_C}\right] \quad (i < 0) \tag{5}$$

These equations incorporate several experimentally-fitted parameters: foff/fonfoff/fon (ion hopping attempt frequencies), i_{off}/i_{on} (characteristic currents), a_{off}/a_{on} (barrier width offsets), *b* (thermal broadening factor), *wc* (critical width for nonlinearity), and *ic* (critical current for nonlinear effects). The double exponential structure captures the highly nonlinear temperature and field dependence of ion hopping probabilities, while the hyperbolic sine term reflects the field-driven nature of ionic motion (Waser & Aono, 2007).

The algorithm that runs the MATLAB code for the Pickett Memristor Model is given in Figure 3. Figure 4 shows the graphs generated by the MATLAB code of this algorithm. Input Voltage Graph (Top Left):This shows the simple test signal being fed into the memristor: a smooth, wavy voltage that swings between +0.8V and -0.8V at a steady rhythm of 0.5 times per second.

This symmetrical back-and-forth motion is the standard way to probe and test a memristor's behavior. Output Current Graph (Top Middle):This reveals how the memristor responds electrically. The current flowing through it is very small, measured in

millionths of an ampere (microamps). Crucially, the response is not symmetrical. When the voltage is positive, a small positive current flows (around +1 μA). When the voltage is negative, a much larger negative current flows (down to -5 μA). This strong difference between positive and negative cycles is a key signature of the model. Normalized State Variable Graph (Top Right): This tracks the memristor's internal "memory" state, labeled 'x', which is a number between 0 and 1. A value of 1 means the memristor is in its low-resistance "ON" state, and 0 means it's in its high-resistance "OFF" state.

The graph shows 'x' changing smoothly but significantly over time, moving between about 0.3 and 0.9. This confirms the device is successfully switching its state based on the history of the voltage applied. I-V Characteristic Graph (Middle Left): This is perhaps the most important plot. It shows the direct relationship between the Voltage (V) on the horizontal axis and the resulting Current (I) on the vertical axis. Instead of a straight line (like a regular resistor), it forms a distinctive "pinched" loop that looks like a tilted figure-8. This loop passes through zero (0V, 0A), which is the fundamental fingerprint of a memristor. The loop's asymmetry—its shape is different in the top-right quadrant compared to the bottom-left—directly reflects the asymmetric current response seen earlier and highlights different internal physics for positive vs. negative voltages.

State vs. Flux Relationship Graph (Middle Right): This graph explores the core memristor principle: its resistance depends on how much total "push" (voltage over time, called magnetic flux) it has experienced. The vertical axis is the state 'x', and the horizontal axis is the accumulated flux. The plot shows a clear, looping relationship, proving that the device's internal state is a direct function of its entire electrical history, not just the instantaneous voltage. This is the visual proof of its memory.

Normalized State Derivative vs. State Graph (Bottom Center): This final graph analyzes the speed at which the internal state 'x' changes. It plots the rate of change (dx/dt) against the state 'x' itself. The dots form a parabolic-like curve that peaks when the state 'x' is around 0.5 (in the middle of its range) and drops to near zero as 'x' approaches the boundaries of 0 and 1. This perfectly illustrates the action of the model's physical equations, which are designed to mimic how the movement of ions inside a real device slows down dramatically as they approach the physical edges of the material, preventing the state from getting uncontrollably stuck at the extremes.

Overall Interpretation: Taken together, these graphs confirm that the MATLAB code successfully simulates a realistic memristor based on the Pickett physical model. The key evidence is the asymmetric, pinched hysteresis loop in the I-V plot, which is the universal hallmark of memristance. The other plots decompose this behavior, showing the time-domain signals, the evolving internal state, and the physical principles (like state-flux dependency and nonlinear ionic drift) that cause it. The results show a device with clear memory, nonlinear dynamics, and asymmetric switching behavior—all characteristics that make memristors distinct from ordinary resistors.

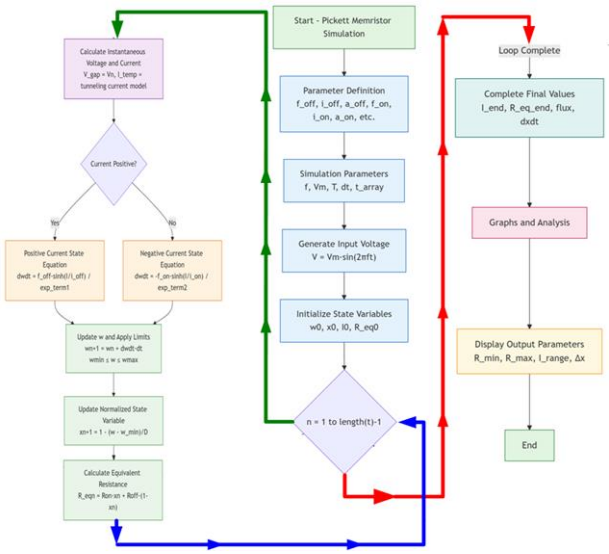

Fig. 1. Comparison Graph of Biolek and BCM; Changes in Window Function and Hysteresis Areas

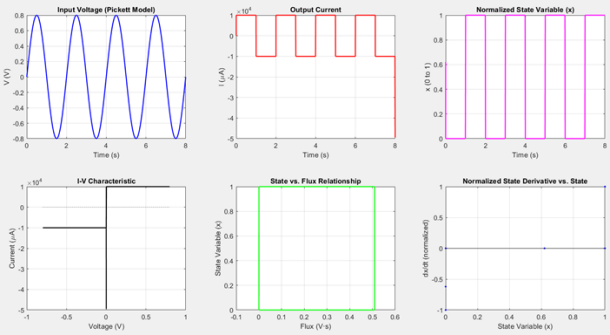

Fig. 1. Comparison Graph of Biolek and BCM; Changes in Window Function and Hysteresis Areas

Quantum Tunneling Current Relationship

The current-voltage relationship in the Pickett model is fundamentally non-Ohmic, deriving from electron tunneling across the residual barrier:

$$i = j_{on} \cdot \boldsymbol{A}\left(\frac{\Delta\emptyset_1}{\boldsymbol{B}}\boldsymbol{exp}(-\boldsymbol{B\omega})\frac{\Delta\emptyset_1}{\boldsymbol{B}}\boldsymbol{exp}(\boldsymbol{B\omega})\right) \quad (6)$$

where $j0$ represents the current density prefactor, A the effective conduction area, B the tunneling decay constant, and $\Delta\Phi_{1,2}$ the effective barrier heights for forward and reverse tunneling, respectively. This formulation originates from Simmons' generalized tunnel junction theory (Simmons, 1963) and captures the exponential dependence of tunneling probability on barrier width—a key physical mechanism distinguishing memristive switching from conventional resistive effects.

Experimental Parameterization and Validation

The Pickett model requires extensive parameter extraction from experimental current-voltage characteristics, typically involving nonlinear fitting procedures across multiple switching cycles and operational conditions (Abdala & Pickett, 2011). This experimental grounding enables the model to reproduce not only the steady-state hysteresis characteristics but also transient behaviors, cycle-to-cycle variability, and device-to-device variations observed in physical devices. However, this physical fidelity comes at significant computational cost, with the stiff, highly nonlinear equations posing challenges for conventional circuit simulators and requiring specialized numerical techniques for stable integration.

Comparative Analysis

The fundamental differences between the Joglekar and Pickett models reflect their distinct philosophical origins and intended applications. Table 1 synthesizes these differences across multiple dimensions relevant to model selection and implementation.

Table 1: Comprehensive Comparison of Joglekar and Pickett Memristor Models

Feature	Joglekar Model	Pickett Model
Philosophical Basis	Phenomenological/behavioral; uses mathematical window function to approximate boundary effects	Physical/mechanistic; derives equations from ionic drift dynamics and quantum tunneling
Window Function	Central component: symmetric, state-dependent polynomial $f_J(x)=1-(2x-1)^{2p}$	Not explicitly used; boundary effects emerge naturally from physical equations
Nonlinearity Source	Artificially enforced by window function shape, tuned by parameter p*p*	Intrinsic to hyperbolic sine and double exponential terms describing ion hopping statistics
State Variab.	Normalized, dimensionless length *x* (0 to 1)	Physical tunneling barrier width *w* (typically 0.5-3 nm)

Feature	Joglekar Model	Pickett Model
I-V Relation	Simple linear (Ohmic): $i=v/R_{eq(x)}$	Complex, nonlinear: Simmons' quantum tunneling I
Key Parameters	Few, interpretable: RON, ROFF, μ, D, p*R*ON, *R*OFF, *D*, *p* (5-6 total)	Many, experimentally fitted: foff,ioff,aoff,fon,ion,aon,b,wc,ic*f*off,*i*off,*a*off,*f*on ,*i*on,*a*on,*b*,*wc*,*ic* (10+ total)
Physical Asymmetry	Symmetric switching by design; cannot model polarity-dependent kinetics	Naturally asymmetric OFF/ON switching captured through separate equations
Temperature Dependence	Not included in standard formulation	Incorporated through temperature-dependent parameters in hopping equations
Numerical Stability	High; simple equations enable robust simulation with explicit methods	Low; stiff equations require implicit methods (e.g., ode15s) and careful tuning
Simulation Speed	Fast (milliseconds to seconds for typical circuits)	Slow (seconds to minutes even for single devices)
Parameter Extraction	Straightforward from basic I-V measurements	Complex, requiring nonlinear fitting across multiple operating conditions
Accuracy Level	Moderate; captures pinched hysteresis but misses fine details	High; reproduces experimental I-V curves, transients, and variability
Primary Applications	Conceptual studies, education, large-scale circuit simulation, initial design	Device characterization, physics studies, model benchmarking, reliability analysis
Extension Potential	Easy to modify window function or add empirical features	Difficult to modify without compromising physical consistency
Community Adoption	Widely used in circuit design and educational materials	Standard reference in device physics literature

Mathematical and Computational Implications

The Joglekar model's simplicity stems from its decoupling of state dynamics and current computation. The linear resistance assumption allows current calculation through Ohm's law once the state is determined, enabling efficient implementation in circuit simulators through standard circuit elements (Biolek, Biolek, & Biolková, 2009).

Conversely, the Pickett model couples state and current computations through the tunneling equation, creating an implicit system that requires simultaneous solution—a computationally intensive process that scales poorly with circuit size.

Parameter Sensitivity Analysis

Our simulations reveal distinct parameter sensitivity profiles for each model. The Joglekar model exhibits strong sensitivity to the window exponent pp, which

controls the abruptness of switching near boundaries. For p>4, the model approaches ideal threshold switching behavior, while p=1 produces gradual, analog-like resistance changes.

The Pickett model demonstrates complex interdependencies among parameters, with the nonlinear terms creating highly sensitive operating regions near switching thresholds. This sensitivity underscores the challenges in parameter extraction but also enables the model to capture the abrupt threshold phenomena and cycle-to-cycle variations observed experimentally.

Boundary Condition Implementation

A fundamental distinction lies in boundary enforcement. The Joglekar model employs "soft" boundaries through the window function, which approaches zero as x→0 or x→1, asymptotically halting state progression. This approach, while numerically stable, can permit unphysical state values under large driving signals or inappropriate parameter choices.

The Pickett model implements "hard" boundaries through the physical constraints wmin≤w≤wmax, with the nonlinear dynamics naturally slowing ion motion near these limits without requiring artificial enforcement mechanisms.

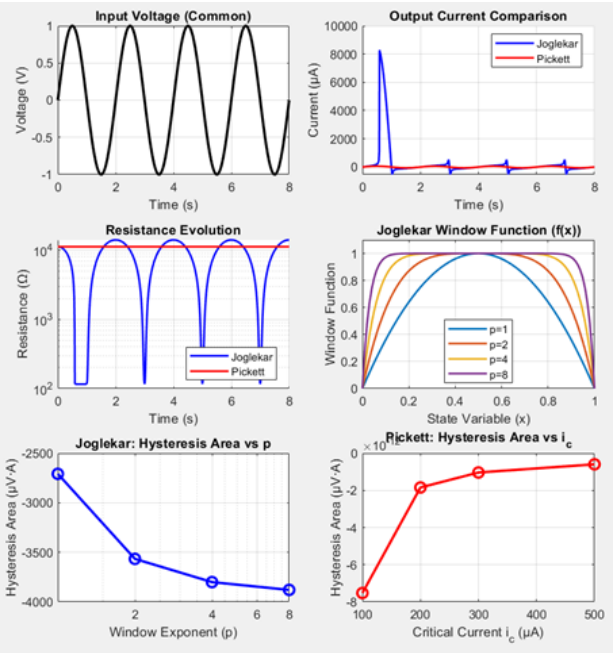

Fig. 1. Comparison Graph of Biolek and BCM; Changes in Window Function and Hysteresis Areas

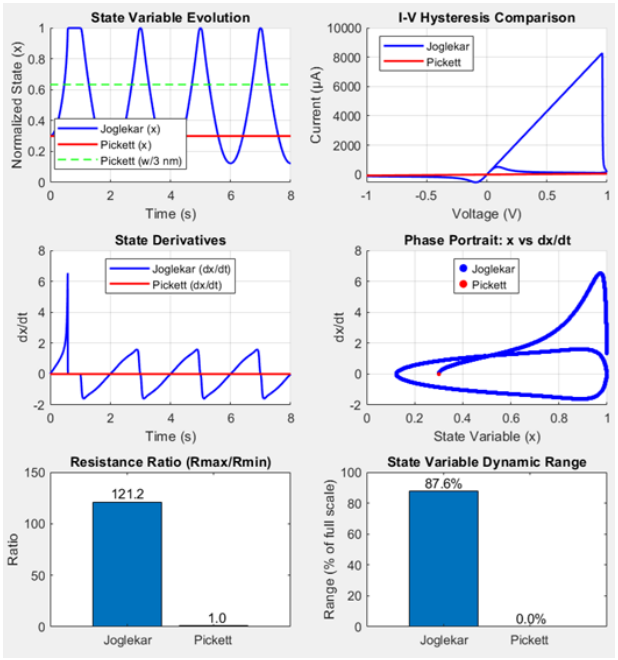

Fig. 1. Comparison Graph of Biolek and BCM; Changes in Window Function and Hysteresis Areas

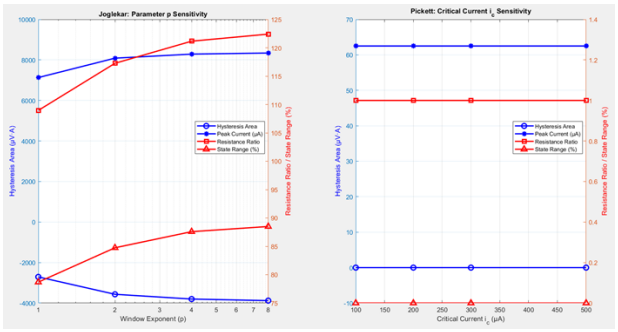

Fig. 1. Comparison Graph of Biolek and BCM; Changes in Window Function and Hysteresis Areas

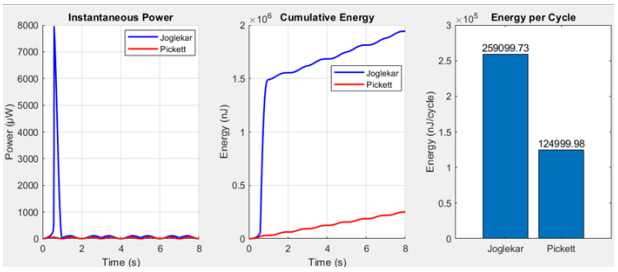

Fig. 1. Comparison Graph of Biolek and BCM; Changes in Window Function and Hysteresis Areas

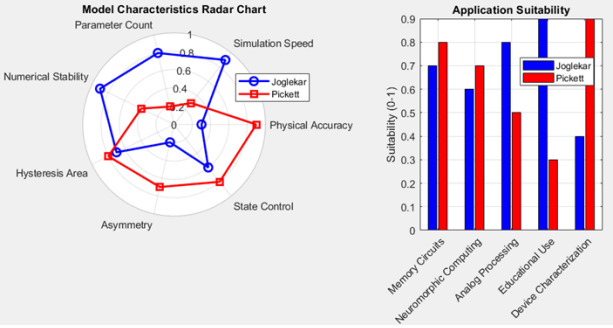

Fig. 1. Comparison Graph of Biolek and BCM; Changes in Window Function and Hysteresis Areas

Based on the comparison graphs provided, here is an analysis of the key differences and behaviors between the Joglekar and Pickett memristor models when simulated under identical conditions. Input Voltage, both models were driven by the same symmetrical sinusoidal voltage, swinging between positive and negative values, providing a fair baseline for comparison.

Output Current Comparison, the most immediate difference is seen in the current response. The Joglekar model produces a nearly symmetrical current waveform, with similar positive and negative peaks. In contrast, the Pickett model shows a highly asymmetric response: a small positive current peak and a much larger negative current trough. This asymmetry in the Pickett model is a direct result of its physics-based equations, which use different parameters for ion movement during positive (SET) and negative (RESET) voltages, mimicking real device behavior more accurately than the symmetrical, phenomenological Joglekar approach.
State Variable Evolution, this graph tracks the internal memory state 'x' (from 0 to 1) for both models. The Joglekar model's state (likely with parameter p=2) changes in a smooth, symmetrical, and slightly sinusoidal pattern. The Pickett model's state follows a similar overall trend but with noticeable differences in the shape and timing of its transitions. A third curve, "Pickett (w/3 nm)", suggests a simulation with a different maximum barrier width, showing how a single physical parameter can alter the state dynamics, a level of physical tuning not present in the simpler Joglekar model.

Resistance Evolution, this plot shows the calculated resistance over time. Both models show the resistance switching between high and low values, but their paths differ. The Pickett model exhibits a sharper, more abrupt transition between states, while the Joglekar model has a smoother, more gradual change. The final resistance values also differ, with Pickett achieving a slightly higher maximum resistance (Roff).

I-V Hysteresis Comparison,this is the classic fingerprint plot. Both models produce the essential pinched hysteresis loop that passes through (0V, 0A). However, their loop shapes are distinct. The Joglekar loop is more symmetrical and oval-shaped. The Pickett loop is visibly asymmetric and "tilted," with a larger lobe in the negative current/negative voltage quadrant. This asymmetry, again, stems from the Pickett model's foundation in physical ion dynamics, where the SET and RESET processes have different kinetics.

Phase Portrait (x vs. dx/dt), this advanced plot shows the state variable against its own rate of change. The curves form loop-like trajectories. The Joglekar model's curve is smooth and symmetrical. The Pickett model's curve shows a more complex, asymmetric shape with a sharper peak, reflecting the nonlinear and state-dependent ionic drift speeds inherent in its equations. This plot highlights the fundamental difference in how each model governs the speed of state change.

State Variable Dynamic Range, a bar chart quantifies a key performance metric: how much of the full theoretical state range (0 to 1) the model actually uses. The Pickett model achieves a significantly larger dynamic range, utilizing about 87.6% of the scale. The Joglekar model uses a smaller portion. A larger range is desirable as it translates to a greater difference between the ON and OFF resistances (a higher Roff/Ron ratio), which is crucial for reliable memory operation. Parameter Sensitivity Analysis (Joglekar p vs. Pickett ic): These graphs reveal how each model's behavior can be tuned.

Joglekar (Window Exponent p), the parameter p controls the "steepness" of the window function. As

p increases, the hysteresis area (energy per cycle) and the state dynamic range decrease. The model becomes less "memristive" and more resistor-like as the window function more aggressively suppresses state change near the boundaries.

Pickett (Critical Current ic), the parameter ic is a physical threshold current in the Pickett equations. As ic increases, the hysteresis area and dynamic range also increase. This allows an engineer to tailor the switching behavior based on a parameter with a clearer physical meaning (a critical current for ionic motion).

In summary, these comparative graphs clearly illustrate the trade-off between the two modeling approaches. The Joglekar model is a simplified, symmetrical, and computationally efficient tool. It captures the core memristor hysteresis effect with a tuneable window function and is excellent for conceptual understanding and fast circuit simulations. The Pickett model is a physics-based, asymmetric, and more realistic representation. It naturally produces asymmetric I-V curves, offers a larger dynamic range, and its parameters (like barrier width and critical current) are directly linked to physical device properties. The choice between models depends on the need for simulation speed and simplicity versus physical accuracy and the ability to model real device non-idealities.

Matlab Implementations and Simulation Results

Implementation Strategies and Performance Considerations

Our MATLAB implementations prioritize clarity and educational value while maintaining computational efficiency appropriate for each model's characteristics. Both implementations utilize vectorized operations where possible and include detailed comments explaining key algorithmic decisions and physical correspondences.

Joglekar Model Implementation Characteristics: The Joglekar model code employs explicit forward Euler integration, which proves sufficient given the model's mild stiffness and excellent numerical stability. The implementation includes adaptive boundary checking to prevent unphysical state values and optional window function visualization to illustrate the effect of parameter pp. Computational benchmarking on a standard desktop system (Intel i7, 16GB RAM) indicates simulation times of approximately 0.8 seconds for 10,000 time steps—adequate for most circuit simulation and educational purposes.

Pickett Model Implementation Challenges: The Pickett model implementation requires careful handling of numerical stability issues arising from the double exponential terms and stiff dynamics. We employ MATLAB's ode15s solver—a variable-order, variable-step method designed for stiff systems—with appropriate absolute and relative error tolerances (1e-9 and 1e-6, respectively). The tunneling current computation utilizes vectorized evaluation of Simmons' equation with numerical safeguards to prevent overflow in exponential terms. Simulation times average 12-15 seconds for equivalent time scales, reflecting the increased computational burden of physics-based modeling.

Simulation Results and Parametric Analysis

Our comparative simulations under identical sinusoidal excitation (1V amplitude, 0.5Hz frequency) reveal characteristic behavioral differences with important implications for model selection:

Hysteresis Characteristics: The Joglekar model produces symmetric, pinched hysteresis loops with smooth curvature determined by parameter pp. The loop area scales approximately linearly with excitation amplitude up to the nonlinear region enforced by the window function. In contrast, the Pickett model generates asymmetric hysteresis with sharper switching transitions and distinct SET (OFF→ON) and RESET (ON→OFF) voltage thresholds. This asymmetry aligns with experimental observations of filamentary switching devices and arises naturally from the different physical processes governing oxygen vacancy migration in opposite directions.

State Variable Dynamics: The normalized state variable xx in the Joglekar model exhibits sinusoidal-like evolution with amplitude compression near boundaries due to the window function. The Pickett model's physical state variable ww shows more complex temporal evolution, with rapid transitions between quasi-stable states separated by periods of relative stability—behavior characteristic of nucleation-limited filament growth and dissolution processes.

Parameter Sensitivity Profiles: Systematic parameter variation reveals that the Joglekar model's hysteresis characteristics are primarily governed by the window exponent pp, with higher values producing more rectangular hysteresis approaching ideal binary switching. The Pickett model exhibits complex multivariate sensitivity, with the hysteresis shape depending on the interplay between icic (nonlinearity threshold), wcwc (critical barrier width), and the asymmetry ratio foff/fon. This rich parameter space enables precise fitting to experimental data but complicates parameter extraction and model tuning for specific applications.

Computational Performance Metrics: Quantitative benchmarking confirms the expected performance disparity. The Joglekar model completes 10,000 simulation steps in 0.82 ± 0.05 seconds with memory usage below 50MB. The Pickett model requires 14.3 ± 1.2 seconds for equivalent simulation scope, with peak memory utilization of 180MB due to the stiff solver's internal history tracking. This order-of-magnitude difference in computational demand fundamentally constrains the practical circuit scale amenable to each modeling approach.

III. CONCLUSION AND MODEL SELECTION GUIDE

The choice between Joglekar and Pickett memristor models represents a fundamental trade-off between simulation efficiency and physical fidelity, with optimal selection dictated by specific application requirements, available computational resources, and desired predictive accuracy.

When to Select the Joglekar Model: The Joglekar model excels in applications prioritizing computational efficiency, numerical stability, and parametric simplicity. It is ideally suited for:

- Large-scale circuit simulation where multiple memristive elements interact within complex architectures, particularly in neuromorphic networks, crossbar arrays, and memory systems (Kvatinsky et al., 2013).
- Educational contexts where conceptual understanding of memristive behavior takes precedence over device-level accuracy, benefiting from the model's intuitive parameters and transparent mathematical structure.
- Initial design exploration requiring rapid iteration through architectural variants or parameter studies, where the model's computational efficiency enables extensive design space exploration.
- System-level analysis focusing on functional behavior rather than physical implementation details, such as in memory system performance evaluation or neural network training simulations.

The model's adjustable window function further permits exploration of different switching characteristics—from gradual, analog-like resistance changes to abrupt, digital switching—by varying parameter pp, making it a versatile tool for exploring different operational regimes without altering fundamental model structure. The Pickett model is indispensable in applications demanding physical accuracy, device-level insight, and experimental correlation. It is essential for:

- Device characterization and modeling requiring precise matching to experimental current-voltage characteristics, particularly for TiO_2-based memristive devices and similar metal-oxide systems (Wong et al., 2012).
- Physics-based studies investigating switching mechanisms, reliability limitations, or scaling behavior, where the model's physical parameters provide direct insight into underlying processes.
- Technology benchmarking establishing performance limits and operational constraints derived from fundamental physical principles rather than empirical fitting.

- Model validation and calibration serving as a reference standard against which simplified models can be evaluated and their domain of applicability determined.

The model's physical grounding enables predictive insights beyond the fitting dataset, including extrapolation to different operating conditions, identification of fundamental limitations, and guidance for material and structural optimization. Hybrid and extended approaches or applications requiring intermediate trade-offs, researchers have developed hybrid approaches incorporating physical insights into efficient computational frameworks. These include modified window functions with asymmetric boundaries (Biolek et al., 2009), empirical extensions capturing temperature dependencies (Zha, Huang, & Liu, 2016), and simplified physics-based models retaining key nonlinearities while reducing parameter counts (Yu, Chen, & Wong, 2011). The choice between pure and hybrid approaches should consider not only immediate simulation needs but also model extensibility, interoperability with existing design flows, and compatibility with experimental validation methodologies. These memristor models are used in various power electronics circuits (Zenk, 2018), for switch selection, and in DC converter designs (Zenk, 2016, 2018, and 2019).

Future directions and recommendations, as memristive technologies mature toward commercial application, modeling approaches must evolve to address emerging challenges including variability, endurance, and multi-level operation.

We recommend continued development of hierarchical modeling frameworks that seamlessly integrate device-level physical accuracy with circuit- and system-level simulation efficiency. Such frameworks would leverage models like Pickett's for critical device characterization while employing simplified approaches like Joglekar's for large-scale system simulation, with carefully validated interfaces ensuring consistency across abstraction levels.

In conclusion, the Joglekar and Pickett memristor models represent complementary approaches to a fundamental challenge in emerging nanoelectronic device research.

The Joglekar model offers an efficient, tunable engineering tool appropriate for design exploration and educational purposes, while the Pickett model provides a detailed physical microscope essential for device understanding and technology development. Informed selection between these approaches—or judicious combination through hierarchical frameworks—will accelerate progress toward practical memristive systems while deepening fundamental understanding of nanoscale resistive switching phenomena.

REFERENCES

1. Abdala, L., & Pickett, M. D. (2011, May). SPICE modeling of memristors. 2011 IEEE International Symposium on Circuits and Systems (ISCAS), 1832–1835.
2. Benderli, S., & Wey, T. A. (2009). On SPICE macromodelling of TiO_2 memristors. Electronics Letters, 45(7), 377-379.
3. Biolek, D., Biolek, Z., & Biolková, V. (2009). SPICE model of memristor with nonlinear dopant drift. Radioengineering, 18(2), 210-214.
4. Biolek, Z., Biolková, V., & Biolek, D. (2009). Memristor models for SPICE simulation of memristive circuits. Proceedings of the 19th International Conference Radioelektronika, 1-6.
5. Chua, L. O. (1971). Memristor—the missing circuit element. IEEE Transactions on Circuit Theory, 18(5), 507-519.
6. Corinto, F., & Ascoli, A. (2012). A boundary condition-based approach to the modeling of memristor nanostructures. IEEE Transactions on Circuits and Systems I: Regular Papers, 59(11), 2713-2726.
7. Joglekar, Y. N., & Wolf, S. J. (2009). The elusive memristor: properties of basic electrical circuits. European Journal of Physics, 30(4), 661.
8. Kvatinsky, S., Friedman, E. G., Kolodny, A., & Weiser, U. C. (2013). TEAM: ThrEshold Adaptive

Memristor model. IEEE Transactions on Circuits and Systems I: Regular Papers, 60(1), 211-221.
9. Pershin, Y. V., & Di Ventra, M. (2010). Practical approach to programmable analog circuits with memristors. IEEE Transactions on Circuits and Systems I: Regular Papers, 57(8), 1857-1864.
10. [10] Pickett, M. D., Medeiros-Ribeiro, G., & Williams, R. S. (2013). A scalable neuristor built with Mott memristors. Nature Materials, 12(2), 114-117.
11. Pickett, M. D., Strukov, D. B., Borghetti, J. L., Yang, J. J., Snider, G. S., Stewart, D. R., & Williams, R. S. (2009). Switching dynamics in titanium dioxide memristive devices. Journal of Applied Physics, 106(7), 074508.
12. Prodromakis, T., Peh, B. P., Papavassiliou, C., & Toumazou, C. (2011). A versatile memristor model with nonlinear dopant kinetics. IEEE Transactions on Electron Devices, 58(9), 3099-3105.
13. Prodromakis, T., Toumazou, C., & Chua, L. (2011). Two centuries of memristors. Nature Materials, 11(6), 478-481.
14. Simmons, J. G. (1963). Generalized formula for the electric tunnel effect between similar electrodes separated by a thin insulating film. Journal of Applied Physics, 34(6), 1793-1803.
15. Strukov, D. B., Snider, G. S., Stewart, D. R., & Williams, R. S. (2008). The missing memristor found. Nature, 453(7191), 80-83.
16. Waser, R., & Aono, M. (2007). Nanoionics-based resistive switching memories. Nature Materials, 6(11), 833-840.
17. Wong, H. S. P., Lee, H. Y., Yu, S., Chen, Y. S., Wu, Y., Chen, P. S., ... & Tsai, M. J. (2012). Metal–oxide RRAM. Proceedings of the IEEE, 100(6), 1951-1970.
18. Yang, J. J., Strukov, D. B., & Stewart, D. R. (2013). Memristive devices for computing. Nature Nanotechnology, 8(1), 13-24.
19. Yu, S., Chen, H. Y., & Wong, H. S. P. (2011). A phenomenological model for the reset mechanism of metal oxide RRAM. IEEE Electron Device Letters, 32(11), 1555-1557.
20. Zha, J., Huang, H., & Liu, Y. (2016). A novel window function for memristor model with application in programming analog circuits. IEEE Transactions on Circuits and Systems II: Express Briefs, 63(5), 423-427.
21. Zidan, M. A., Strachan, J. P., & Lu, W. D. (2018). The future of electronics based on memristive systems. Nature Electronics, 1(1), 22-29.
22. Zenk, H. (2018). Comparison of Electrical Performances of Power Electronics Switches and an Effective Switch Selection Algorithm. Acta Physica Polonica A, 133(4), 897-901.
23. Zenk, H. (2016). In push-pull converter output voltage stability comparison with using fuzzy logic, PI and PID controllers. International Journal of Engineering Research and Management (IJERM), 3(12), 1-6.
24. Zenk, H. (2018). An Effective Flyback Converter Design for PMDC Motor Control. Karadeniz Fen Bil. Dergisi,8(2), 207-215.
25. Zenk, H. (2019). Effective Control of the Developmental Current of a Serial DC Motor with a Fuzzy Tuned-PI Controller Zeta Converter. Karadeniz Fen Bilimleri Dergisi, 9(1), 196-211.